Analysis and Design of Improved Weighted Average Current Control Strategy for LCL-Type Grid-Connected Inverters

Han, Yang; Li, Zipeng; Yang, Ping; Wang, Congling; Xu, Lin; Guerrero, Josep M.

Published in:
I E E E Transactions on Energy Conversion

DOI (link to publication from Publisher):
10.1109/TEC.2017.2669031

Publication date:
2017

Document Version
Early version, also known as pre-print

Analysis and Design of Improved Weighted Average Current Control Strategy for LCL-Type Grid-Connected Inverters

Yang Han, *Member*, *IEEE*, Zipeng Li, Ping Yang, Congling Wang, Lin Xu, and Josep M. Guerrero, *Fellow*, *IEEE*

***Abstract*—The LCL grid-connected inverter has the ability to attenuate the high-frequency current harmonics. However, the inherent resonance of the LCL filter affects the system stability significantly. To damp the resonance effect, the dual-loop current control can be used to stabilize the system. The grid current plus capacitor current feedback system is widely used for its better transient response and high robustness against the grid impedance variations. While the weighted average current (WAC) feedback scheme is capable to provide a wider bandwidth at higher frequencies but show poor stability characteristics under weak grid scenarios. To overcome this shortcoming, the improved WAC damping method is proposed with an additional capacitor current feedback loop. In this paper, a systematic parameter design guideline for the optimal selection of the current loop PR controller and the additional capacitor current feedback coefficient are presented for the improved WAC feedback control strategy. The satisfactory range of the system control parameters can be obtained under different delay conditions to meet the system performance specifications. The improved WAC method enhances system robustness under weak grid scenarios, and the stability and robustness have been enhanced under control delay. Finally, the experimental results are presented to validate the effectiveness of the proposed improved WAC control strategy and the parameter design method.**

***Index Terms*—Active damping, grid-connected PWM inverter, current control, grid impedance, harmonic distortion, weighted average current control.**

NOMENCLATURE

Abbreviations

PCC	Point of common coupling.
WAC	Weighted average current.
PR	Proportional resonant controller.
PLL	Phase-locked loop.
THD	Total harmonic distortion.
HC	Harmonic compensator.
GM	Gain margin.
PM	Phase margin.
$G_{open,igic}$	Open loop transfer function of i_g plus i_c feedback method.
$G_{open,IWAC}$	Open loop transfer function of improved WAC feedback method.
$G_{close,WAC}$	Closed-loop transfer function of WAC feedback method.
$G_{close,IWAC}$	Closed-loop transfer function of improved WAC feedback method.
G_L	Loop gain of improved WAC feedback method.
G_c	Transfer function of PR controller.
G_d	Transfer function of digital control delays.
Variables	
i_{ref}	Reference current.
E_A	Steady state error.
$K_{c,PM}$	K_c constrained by PM
$K_{c,GM}$	K_c constrained by GM
V_{dc}	Amplitude of the input dc-link voltage.
V_{tri}	Amplitude of the triangular carrier.
i_g	Injected grid current.
i_L	*LCL* inverter side current.
i_c	*LCL* capacitor current
K_g, K_L	Sensor gain of grid current and *LCL* inverter side current.
K_c	Active damping coefficient
K_p, K_r	Parameters of the PR controller.
Parameters	
L_1	Inverter-side inductance
L_2	Grid-side inductance
L_g	Equivalent grid inductance
C	Filter capacitor
ω_0, ω_c	Fundamental and cutoff frequencies.
f_r	*LCL* resonance frequency.
T_d	Delay time.
T_s	Sampling and switching period.

Manuscript received July 23, 2016; revised December 27, 2016; accepted February 08, 2017. This work was supported in part by the National Natural Science Foundation of China under Grant 51307015, in part by the Open Research Subject of Sichuan Province Key Laboratory of Power Electronics Energy-Saving Technologies & Equipment under Grant szjj2015-067, in part by the Open Research Subject of Artificial Intelligence Key Laboratory of Sichuan Province under Grant 2015RZJ02, and in part by the Fundamental Research Funds of Central Universities of China under Grant ZYGX2015J087. Paper no. TEC-00619-2016.

Y. Han, Z. Li, P. Yang, and C. Wang are with the Department of Power Electronics, School of Mechatronics Engineering, University of Electronic Science and Technology of China (UESTC), No.2006, Xiyuan Avenue, West Hi-Tech Zone, Chengdu 611731, China (e-mail: hanyang@uestc.edu.cn; zroc.lee@qq.com; ping@uestc.edu.cn; wangcl12@163.com).

L. Xu is with the Sichuan Electric Power Research Institute, Sichuan Electric Power Company, Chengdu 610072, China (xulinn@163.com).

J. M. Guerrero is with Department of Energy Technology, Aalborg University, 9220 Aalborg, Denmark (e-mail: joz@et.aau.dk).

Color versions of one or more of the figures in this paper are available online at http://ieeexplore.ieee.org.

Digital Object Identifier ******/TEC.*******

I. INTRODUCTION

THE increasing global energy consumption has greatly accelerated the demand for renewable energy, such as wind and solar power. The grid-connected PWM inverters play an important role for interconnecting renewable energy and the utility grid [1]. Compared to *L* filter, high order *LCL* filter can

attenuate harmonics produced by the PWM inverter effectively with reduced cost and size, making *LCL* filter an popular solution in industrial applications [2]. However, the resonant peak produced by *LCL*-filter can seriously affect the system stability [3]. In order to stabilize the system, the passive damping scheme by adding a resistor in series with the filter capacitor has been widely adopted for its simplicity and high reliability. But it inevitably leads to higher power losses and decreasing system efficiency [4]. Therefore, the active damping methods which can be achieved by feeding back other control variables as damping terms to the current control loop are preferred due to its efficiency and flexibility [5-8].

Compared with single-loop current control [9], the dual-loop active damping control schemes are preferable which responses slower but with better output waveform quality [10]. Generally, the inner current loop is mainly used for active damping, and the outer grid current loop with current controller is used for tracking the reference current, and in synchronism with the voltage at the point of common coupling (PCC) [11],[12]. In retrospect, the grid current plus *LCL* capacitor current feedback control scheme was widely addressed [6], [10], [13-16]. And proportional feedback of the capacitor current has been proven to be equivalent to a virtual resistor connected in parallel with the filter capacitor [16]. In addition to *LCL* capacitor current, *LCL* inverter side current can also be used as the inner control variable [11], [17]. And it was mentioned in [14] that, from the dynamic point of view, the capacitor current plus grid current feedback control scheme is equivalent to the converter current plus grid current feedback control scheme.

On the other hand, the weighted average current (WAC) control method was derived by combing the conventional single converter current feedback and grid current feedback loops, which has been successfully introduced in the *LCL* grid connected inverter to damp the resonance [18, 19]. With this approach, the order of the system transfer function can be degraded from a third-order function to a first-order one [19], the current harmonics can be decreased and the dynamic performance can also be enhanced. A comparative analysis between two current sensor feedback methods was presented in [20], and it is found that the WAC control has high controller bandwidth but more sensitive to the *LCL* inductor variation, which may make the system unstable. Moreover, when the weighted average current is controlled, both the grid-side current and the inverter-side inductor current are critically stable even though the weighted average current can be easily stabilized [21].

In [22], an improved current feedback control method combined with the WAC feedback and capacitor current feedback is proposed. In the proposed control scheme, the capacitor current feedback is introduced at the inner loop without adding any extra current sensor. Consequently, the resonance damping and harmonic suppressing capability are improved. Besides, the improved WAC method is also capable of reducing the sensitivity to the disturbance and improving the quality of the grid current. However, in the WAC control method, only the weighted current is directly controlled, thus the injected grid current may have a steady state error at the output, which affects the system performance significantly. Besides, the *LCL*-filter resonance frequency will vary in a wide range due to the variation of the grid impedance, which challenges the design of capacitor current feedback coefficient and the current controller parameters [23, 24].

Based on the concept of the virtual resistor, a step-by-step method was proposed in [15] to design the active damping coefficient and the current control parameters of the grid current plus capacitor current feedback control method. This design method is useful when the delay effect is ignored, but the digital control delay is inevitable in the digital-controlled system and will change the system phase-frequency characteristic, thus the system stability will be affected [25, 26]. Therefore, the delay effect should be considered in the design procedure to determine the capacitor-current-feedback coefficient and the current controller parameters. However, the parameter design guidelines for the improved WAC control scheme has not been reported in the existing literatures.

The main contributions of this paper are summarized as follows.

1) This paper presents the comparison between the grid current plus capacitor current feedback method and the improved WAC feedback method. It was proved that with improved WAC feedback control method, a lager current controller proportional gain can be adopted to provide larger bandwidth at higher frequencies, and the system robustness under weak grid conditions can be enhanced.

2) A systematic method for designing PR controller and the capacitor current feedback coefficient are presented for the improved WAC feedback control scheme under different delay conditions. With this method, controller parameters and the active damping feedback coefficient can be easily obtained by specifying the system stability and dynamic performance indices, and it is more convenient and explicit to optimize the system performance according to the satisfactory region. The improved WAC method enhances system robustness under weak grid conditions, and the system becomes more robust against time delay.

3) Implementation of the improved WAC control strategy on a 2.2 kW three-phase experimental platform based on Dansfoss inverter has been presented. The control strategy, designed control parameters and system performance under weak grid and maximum delay time scenario are tested. The results are consistent with the simulation results.

This paper is organized as follows. In Section II, the modeling and analysis for dual-loop current control methods are presented. In Section III, a systematic method for designing PR controller and the capacitor current feedback coefficient in the improved WAC feedback control scheme is presented. The experimental results in Section IV validates the proposed control scheme and parameter design method. Finally, Section V concludes this paper.

II. Modeling And Analysis of The Dual-Loop Current Control Scheme

Fig. 1(a) shows the main circuit of the three-phase *LCL* interfaced grid-connected inverter. L_1, L_2 and L_g represents the inverter-side inductance, the grid-side inductance and the equivalent grid inductance. The voltages at the PCC are sampled for the feed-forward loop and the phase-locked-loop (PLL). The corresponding current control diagram is shown in Fig. 1(b), where K_{pwm} is the transfer function of the PWM

inverter, which is defined as V_{dc}/V_{tri}, where V_{dc} is the amplitude of the input dc-link voltage and V_{tri} is the amplitude of the triangular carrier [15]. The injected grid current i_g and the *LCL* inverter side current i_L are sensed with the sensor gain K_g and K_L respectively. The gain K_g and K_L are equal to $L_2/(L_1+L_2)$ and $L_1/(L_1+L_2)$ respectively. A novel feedback variable i_{wac} named weighted current has been constructed.

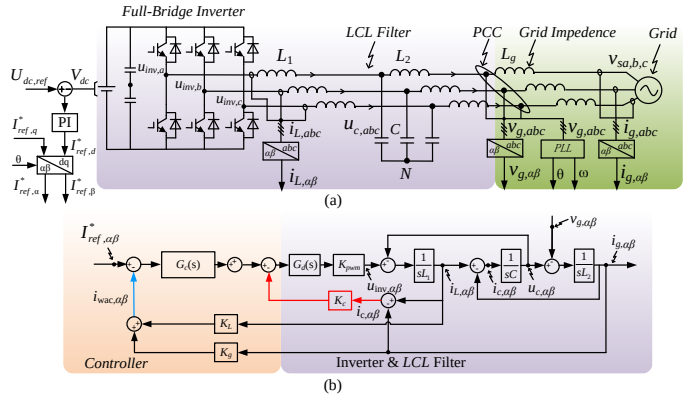

Fig. 1. Three-phase grid-connected inverter with an LCL filter in stationary α – β frame. (a) Main circuit. (b) Control diagram.

The inner capacitor current i_c feedback introduces the active damping to damp the *LCL* resonance. G_c(s) is the transfer function of the outer loop controller. And the proportional resonant (PR) regulator is introduced to eliminate the steady state error at the fundamental frequency. To simplify the analysis, the PR controller at the fundamental frequency is given by

$$G_c(s) = K_p\left(1 + K_r \frac{2\omega_c s}{s^2 + 2\omega_c s + \omega_0^2}\right) \tag{1}$$

where K_p is the proportional gain, K_r is the integral gain at the fundamental frequency f_0, ω_0 is the fundamental frequency and ω_c is the bandwidth of the resonant part concerning -3 dB cutoff frequency.

The resonance frequency of the *LCL* filter f_r is written as

$$f_r = \frac{1}{2\pi}\sqrt{\frac{L_1 + L_2}{L_1 L_2 C}} \tag{2}$$

The digitally controlled system contains the computation delay, sampler continuous approximation, and PWM delay [27], which can be expressed as

$$G_d(s) = e^{-s \cdot T_d} \tag{3}$$

The delay effect with three typical values for T_d can be used, with T_d=T_s/2 is defined as the minimum delay, with T_d=T_s defined as the medium delay and with T_d=3T_s/s defined as the maximum delay.

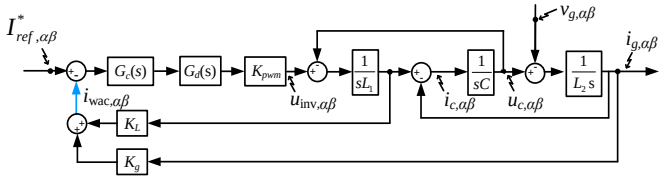

Fig. 2. The s-domain block diagrams of traditional WAC feedback control scheme.

The s-domain block diagrams of traditional WAC feedback control scheme is shown in Fig. 2. From Fig. 2, the close-loop transfer function from the reference current i_{ref} to grid current i_g is expressed as (4), where the subscript "WAC" represents the transfer function with traditional WAC control.

$$G_{close,\mathrm{WAC}}(s) = \frac{D_1}{s^3 C L_1 L_2 + s^2 C L_2 K_L D_1 + s(L_1 + L_2) + D_1} \tag{4}$$

where the parameters D_1 is denoted as

$$D_1 = G_d(s) K_{PWM} G_c(s) \tag{5}$$

Using the parameters listed in Table I [14], Fig. 3 shows the close-loop characteristics of the traditional WAC control method, where K_p is the proportional gain in the current controller. As can be seen from Fig. 3, with the increase of K_p, the system bandwidth is improved. However, the peak at resonant frequency is also increased. As a result, if the noise disturbances especially those around f_r are in existence, the resonance at harmonic frequencies will be amplified. Therefore, the WAC control method needs to be improved. To damp the

TABLE I
PARAMETERS OF THE THREE-PHASE INVERTER

Parameter	Symbol	Values
Dc-link voltage	V_{dc}	650 V
Grid voltage(RMS)	$V_{s,a,b,c}$	220 V
Amplitude of triangle carrier wave	V_{tri}	1 pu
Grid frequency	f_0	50 Hz
Inverter side inductance	L_1	1800 μH
Grid side inductance	L_2	1800 μH
Filter capacitance	C	25 uF
Sampling and switching period	T_s	100 μs
Fundamental angular frequency	ω_0	100π rad/s
Resonance frequency	f_r	1.06 kHz
Switching frequency	f_s	10 kHz

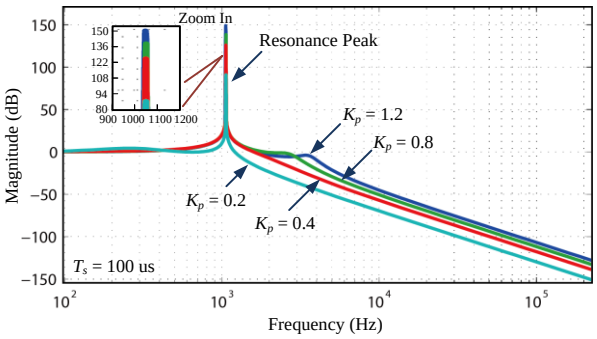

Fig. 3. Amplitude frequency characteristics of the traditional WAC close-loop transfer function (Undamped system).

LCL-resonance, the passive damping method can be used with a resistor in series with the capacitor. This method is simple and effective, but also result in additional power losses.

Conventional WAC feedback system shows a high controller bandwidth but the system robustness under *LCL* parameter variation is poor with a high steady state error [20]. The i_c plus i_g feedback scheme shows a high robustness against the grid impedance variations [28]. However, the controller bandwidth is affected. The improved control method using a combination of the WAC and the capacitor current feedback is shown in Fig.4. Note that the active damping feedback of i_c is obtained using the difference of i_L and i_g according to Kirchhoff's current law, thus an additional high-precision current sensor can be avoided in order to reduce the hardware cost.

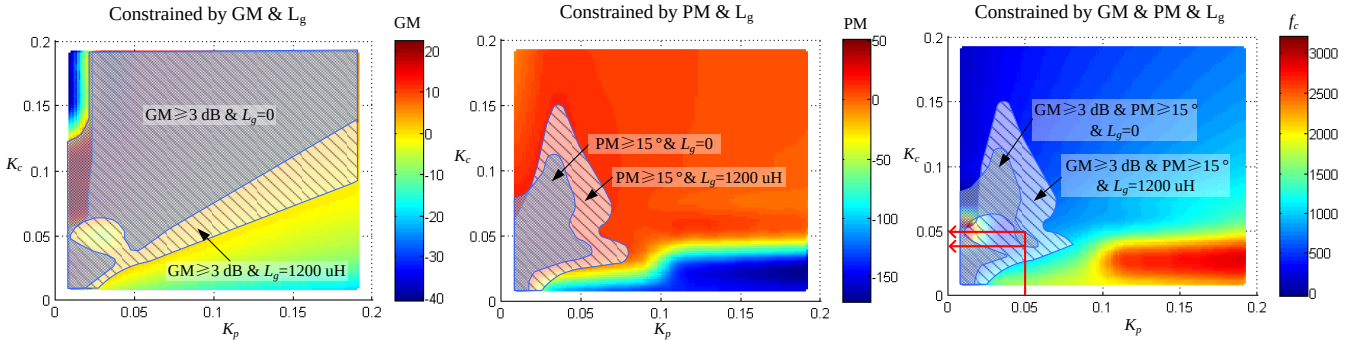

Fig. 7. PM, GM and f_c of i_g plus i_c feedback system. (a) Relationship between K_p, K_c and GM. (b) Relationship between K_p, K_c and PM. (c) Relationship between K_p, K_c and f_c.

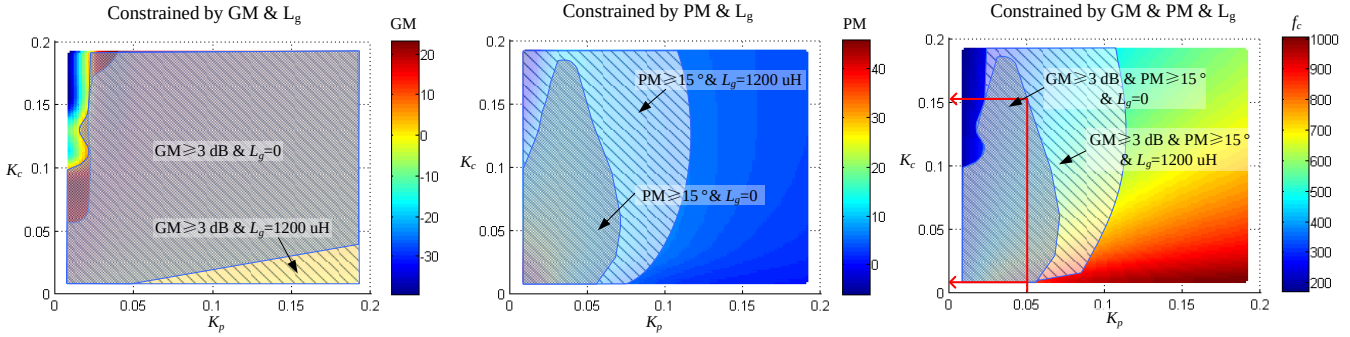

Fig. 8. PM, GM and f_c of improved WAC feedback system. (a) Relationship between K_p, K_c and GM. (b) Relationship between K_p, K_c and PM. (c) Relationship between K_p, K_c and f_c.

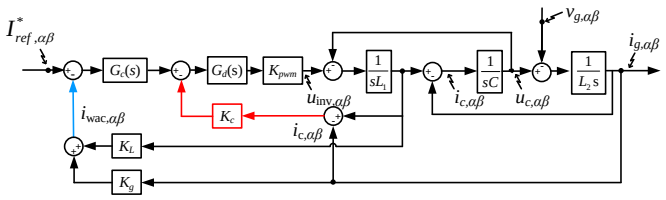

Fig. 4. The s-domain block diagrams of improved WAC feedback control scheme.

From Fig.4, the close-loop transfer function from the reference current i_{ref} to grid current i_g is given in (6), where the subscript "IWAC" represents the transfer function with the improved WAC control method.

$$G_{close,\mathrm{IWAC}}(s)=\frac{D_1}{s^3CL_1L_2+s^2D_2+s(L_1+L_2)+D_1} \tag{6}$$

where the parameter D_2 is denoted as:

$$D_2=CL_2G_d(s)K_{PWM}(K_c+K_LG_c(s)) \tag{7}$$

From (6), the close-loop amplitude frequency characteristics with a variation of K_c are shown in Fig. 5.

As can be seen from Fig. 5, with the increasing of K_c, the resonance peak can be highly suppressed. Besides, the low-frequency response and high-frequency harmonic attenuation ratio are almost unaffected, thus the system stability can be improved without deteriorating high frequency performance.

To compare with the simple i_g plus i_c feedback method and present the merits of the improved weighted average current control strategy. Fig.6 shows the block diagram of i_g plus i_c feedback method in $\alpha\beta$ stationary frame.

When designing the controller, a larger K_p means a faster dynamic response and a larger loop gain at low frequencies, but too large K_p also makes the system unstable. Compared with K_p, a larger K_r results in a larger gain at the fundamental frequency, but the value of K_r has no effects on the system bandwidth. When the feedback loop of the LCL filter capacitor current is introduced, a higher value of K_c shows the better resonance damping capability.

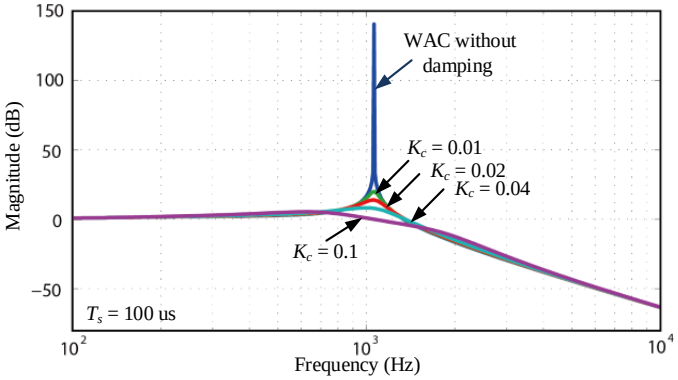

Fig. 5. Amplitude frequency characteristics of the improved WAC close-loop transfer function with additional capacitor current feedback (damped system).

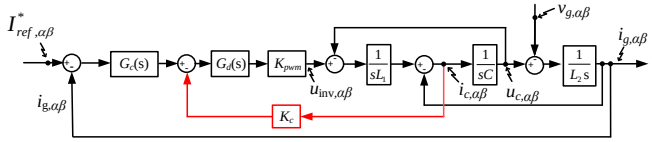

Fig. 6 The s-domain block diagrams of I_g plus I_c dual-loop feedback control scheme [17].

However, too large of K_c has significant impact on the phase of the open loop transfer function and reduces the phase margin. Therefore, the parameter selection of K_p and K_c are of vital significance when designing the current loop, which is described as follows.

The main goals of the current control are to minimize the steady-state error, achieve the best dynamic performance and minimize the harmonics in the injected grid current. Generally, these system performance and stability margin can be specified by steady state error (E_A), crossover frequency (f_c), gain margin (GM) and phase margin (PM) of the system. In general, GM ≥ 3 dB is adopted to ensure the system robust stability, and PM≥15° is adopted to achieve good dynamic response and robustness.

To make a comparison between i_g plus i_c feedback control and improved WAC feedback control, the open loop transfer functions of two feedback system are given in (8) and (9), where the subscript "igic" represents the transfer function with grid current plus capacitor current control.

$$G_{open,\text{igic}}(s)=\frac{G_d(s)K_{PWM}G_c(s)}{s^3CL_1L_2+s^2CL_2G_d(s)K_{PWM}K_c+s(L_1+L_2)} \quad (8)$$

$$G_{open,\text{IWAC}}(s)=\frac{D_1}{s^3CL_1L_2+s^2D_2+s(L_1+L_2)} \quad (9)$$

The value of K_p and K_c can both affect GM, PM and f_c of the system, in order to get the appropriate values of K_p and K_c to achieve the best dynamic performance and ensure system stability. According to (8) and (9), PM, GM and f_c constrained by K_p and K_c can be represented in 3-D plots shown in Fig. 7 and Fig. 8.

As for the i_g plus i_c feedback control system, Fig. 7(a) shows the relationship between K_p, K_c and GM, the possible K_p and K_c that satisfy GM ≥ 3 dB are included in the shaded area. Fig. 7(b) shows the relationship between K_p, K_c and PM, the possible K_p and K_c that satisfy PM ≥ 15° are included in the shaded area. Take into account both GM and PM, the shaded area of K_p and K_c that both satisfying the aforementioned GM and PM are plotted in Fig. 7(c). From Fig. 7(c), a larger f_c can be chosen to achieve a better dynamic performance.

Using the same main circuit parameters, the corresponding plots of the improved WAC feedback system are shown in Fig. 8. Compared with Fig. 7, it can be seen that a larger range of K_p and K_c can be chosen to satisfy GM ≥ 3 dB and PM ≥ 15° with the improved WAC feedback control. For example, if K_p=0.05 is adopted, in i_g plus i_c feedback control system, K_c can be selected in the range of 0.04~0.05. However, in improved WAC feedback control system, K_c can be selected in the range of 0.01~0.15. Similarly, with the same K_c, a larger K_p can be adopted in the improved WAC feedback control system to provide larger bandwidth at higher frequencies.

Under weak grid scenario, the grid impedance L_g is inductive and can be regarded as equivalent to the increasing of inductor L_2. In this study, L_g is increased to 1200 μH to emulate the weak grid condition. When L_g=1200 μH, the areas that satisfying GM ≥ 3 dB and PM ≥ 15° are depicted in Fig. 7 and Fig. 8. It can be seen that the shaded areas of two control methods are both enlarged with larger grid impedance, and the enlarged area of improved WAC control is much larger than that of i_g plus i_c feedback control. Therefore, compared with i_g plus i_c feedback control scheme, the improved WAC method enhances system robustness under weak grid conditions.

III. Parameter Design Guidelines of the Improved WAC Control Scheme

The improved control method contains a combination of the WAC and the capacitor current feedback loops. In order to achieve satisfactory active damping performance, parameter design procedures are of vital significance, which are outlined in this section.

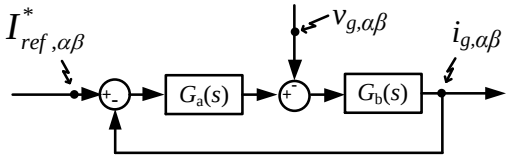

Fig. 9. The equivalent transformation of s-domain block diagrams of the proposed improved WAC feedback control scheme.

The simplified equivalent results are shown in Fig.9, where $G_a(s)$ and $G_b(s)$ are denoted as:

$$G_a(s)=\frac{G_d(s)K_{PWM}G_c(s)}{s^2CL_1+sCG_d(s)K_{PWM}(K_c+K_LG_c(s))+1} \quad (10)$$

$$G_b(s)=\frac{s^2CL_1+sCG_d(s)K_{PWM}(K_c+K_LG_c(s))+1}{s^3CL_1L_2+s^2D_2+s(L_1+L_2)} \quad (11)$$

If the control parameters K_g and K_L are equal to $L_2/(L_1+L_2)$ and $L_1/(L_1+L_2)$, respectively, the system model with *LCL* filter can be degraded from a third-order to a first-order system.

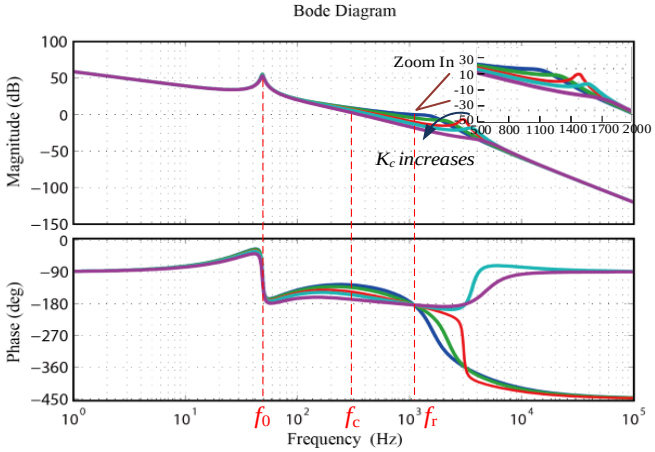

Fig. 10. Bode diagram of the improved WAC control scheme with different capacitor current feedback coefficients.

The loop gain is defined as $G_L(s)$, and can be expressed as

$$G_L(s)=G_a(s)G_b(s)=\frac{G_c(s)G_d(s)K_{PWM}}{s^3CL_1L_2+s^2D_2+s(L_1+L_2)} \quad (12)$$

From the loop gain $G_L(s)$ defined in (12), the bode plot with different capacitor current coefficient is illustrated in Fig. 10. As can be seen from Fig. 10, with additional capacitor current feedback, the system amplitude frequency characteristics above the fundamental frequency can be modified. The magnitude curve crosses over 0 dB at f_c, thus the phase at f_c should be adjusted above -180° to ensure PM>0, and the PM of the system can be expressed as

$$\text{PM}=180^\circ+\angle G_L(s)\big|_{s=j2\pi f_c} \quad (13)$$

In Fig. 10, the phase curve crosses over -180° at the resonance frequency f_r. Therefore, the gain at f_r needs to be adjusted below 0 dB to ensure GM >0. The gain margin GM

can be expressed as

$$\mathrm{GM} = -20\lg\left|G_L(j2\pi f_r)\right| \tag{14}$$

The influence of the filter capacitor can be ignored when calculating the magnitude of the loop gain lower or equal to f_c. Thus $G_L(s)$ and $G_b(s)$ can be approximated as

$$G_L(\mathrm{s}) \approx T(s) = \frac{G_c(\mathrm{s})G_d(\mathrm{s})K_{PWM}}{s(L_1+L_2)} \tag{15}$$

$$G_b(\mathrm{s}) \approx T_2(s) = \frac{1}{s(L_1+L_2)} \tag{16}$$

where $T(s)$ and $T_2(s)$ are the approximation of $G_L(s)$ and $G_b(s)$ respectively. Therefore, with reference to Fig.9, the current injected into the grid can be approximated as

$$i_g(\mathrm{s}) = \frac{T(s)}{1+T(s)} i_{ref}(s) - \frac{T_2(s)}{1+T(s)} v_g(s) \tag{17}$$

where i_{ref} (s)is the reference current and v_g(s) is the grid voltage.

The steady-state error of the grid-connected inverter includes the amplitude error E_A and the phase error δ. The PR controller can eliminate the static error at the fundamental frequency, thus the phase error δ can be attenuated. Considering $T(s) \gg 1$ and $|G_d(j2\pi f_0)| \approx 1$, the amplitude of the grid current i_g at the fundamental frequency f_0 can be expressed as

$$i_g(j2\pi f_0) \approx i_{ref}(j2\pi f_0) - \frac{T_2(j2\pi f_0)}{T(j2\pi f_0)} v_g(s) \tag{18}$$

and the amplitude error E_A can be expressed as

$$E_A = \frac{\left|\left|i_g(j2\pi f_0)\right| - i_{ref}\right|}{i_{ref}} \approx \left|\frac{1}{G_c(j2\pi f_0)}\right| \frac{V_g}{I_{ref}K_{PWM}} \tag{19}$$

where I_{ref} and V_g are the root mean square (rms) values.

At the fundamental frequency f_0, the PR controller can be approximated as

$$G_c(j2\pi f_0) \approx K_p + K_r \tag{20}$$

Substituting (20) into (19) yields

$$K_{r,EA} = \frac{V_g}{E_A I_{ref} K_{PWM}} - K_p \tag{21}$$

where $K_{r,EA}$ is the critical value of the integral gain constrained by E_A. The magnitude of the PR controller can be approximated to K_p at the frequencies equal or higher than f_c, the magnitude frequency response of the system is zero at f_c. Therefore, considering $G_c(j2\pi f_c) \approx K_p$ and $|T(j2\pi f_c)| = 1$, the proportional gain K_p can be written as

$$K_P \approx \frac{2\pi f_c(L_1+L_2)}{K_{PWM}} \tag{22}$$

From (22), it can be inferred that K_p is proportional to f_c, and a larger K_p ensures a faster dynamic response. When the expected crossover frequency f_c is selected, the proportional gain K_p can be determined.

Since f_c is higher than both f_0 and ω_c/π, $G_c(s) \approx K_p + 2K_r\omega_c/s$ is reasonable to calculate the phase margin [15]. Substituting s = $j2\pi f_c$ into $G_L(s)$ in (15), the PM can be rewritten as

$$\begin{aligned}\mathrm{PM} = {} & -180^{\circ} + \arctan\frac{\pi f_c K_P}{K_r\omega_c} \\ & - \arctan\frac{\left[\frac{f_c K_{PWM}K_c}{2\pi L_1} + \frac{f_c K_{PWM}K_P}{4\pi L_1} + 2\pi f_c T_d(f_r^2 - f_c^2)\right]}{\frac{K_{PWM}K_r\omega_c}{2\pi^2 L_1} + f_r^2 - f_c^2}\end{aligned} \tag{23}$$

Equation (23) can be rewritten as

$$K_r^2 G_A + K_r G_B + G_C = 0 \tag{24}$$

where G_A, G_B and G_C are denoted as

$$\begin{aligned} G_A &= \tan(\mathrm{PM}+180^{\circ})\frac{K_{PWM}\omega_c}{2\pi^2 L_1} \\ G_B &= \tan(\mathrm{PM}+180^{\circ})(f_r^2 - f_c^2) - \frac{f_c K_P K_{PWM}}{2\pi L_1} \\ &\quad - f_c\left[\frac{K_{PWM}K_c}{2\pi L_1} + \frac{K_{PWM}K_P}{4\pi L_1} + 2\pi T_d(f_r^2 - f_c^2)\right] \\ G_C &= \tan(\mathrm{PM}+180^{\circ})\frac{\pi f_c^2 K_P}{\omega_c} \\ &\quad \cdot\left[\frac{K_{PWM}K_c}{2\pi L_1} + \frac{K_{PWM}K_P}{4\pi L_1} + 2\pi T_d(f_r^2 - f_c^2)\right] \\ &\quad - \frac{\pi f_c K_P}{\omega_c}(f_r^2 - f_c^2) \end{aligned} \tag{25}$$

Solving (25), the roots of K_r can be expressed as

$$K_{r,1} = \frac{-G_B + \sqrt{G_B^2 - 4G_A G_C}}{2G_A} \tag{26}$$

$$K_{r,2} = \frac{-G_B - \sqrt{G_B^2 - 4G_A G_C}}{2G_A} \tag{27}$$

As K_r>0, the root $K_{r,2}$ is invalid, substituting (19) and (20) into $K_{r,1}$, the boundaries of K_c constrained by PM and E_A can be derived by (28), at the bottom of this page, and the subscript "PM" represents the K_c constrained by PM.

In (28), G_D and G_E are denoted as:

$$\begin{aligned} G_D &= \frac{V_g}{E_A I_{ref} K_{PWM}} - \frac{2\pi f_c(L_1+L_2)}{K_{PWM}} \\ G_E &= \tan(\mathrm{PM}+180^{\circ})(f_r^2 - f_c^2) \\ &\quad - \frac{3f_c^2(L_1+L_2)}{2L_1} - 2\pi f_c T_d(f_r^2 - f_c^2) \end{aligned} \tag{29}$$

In general, the crossover frequency is set over a decade above the fundamental frequency f_0. Therefore, the PR controller can be approximated to K_p around f_c. Considering $|G_d(s)|$=1, and substituting s=$j2\pi f_r$ into (14) yields

$$K_{c,\mathrm{GM}} = \frac{2\pi f_c L_1 10^{\frac{\mathrm{GM}}{20}} - 4\pi^3 f_r^2 f_c L_2 L_1 C}{K_{PWM}} \tag{30}$$

where the subscript "GM" represents the K_c constrained by GM.

$$K_{c,\mathrm{PM}} = \frac{G_D^2 G_A + 4G_D G_E + \tan(\mathrm{PM}+180^{\circ})\frac{2\pi^2 f_c^3(L_1+L_2)}{K_{PWM}\omega_c}\left[\frac{f_c(L_1+L_2)}{2L_1} + 2\pi T_d(f_r^2 - f_c^2)\right] - \frac{2\pi^2 f_c^2(L_1+L_2)}{K_{PWM}\omega_c}(f_r^2 - f_c^2)}{4G_D\frac{K_{PWM}f_c}{2\pi L_1} - \tan(\mathrm{PM}+180^{\circ})\frac{\pi f_c^3(L_1+L_2)}{\omega_c L_1}} \tag{28}$$

From the above analysis, a design method can be obtained:

(*i*) If the upper and lower boundaries of GM and PM, and E_A are specified, the satisfactory region constrained by K_c and f_c can be obtained from (28) and (30).

(*ii*) With the possible value of f_c and K_c, the proportional gain K_P can be calculated from (22).

(*iii*) Finally, with the obtained K_P, the integral gain K_r can be calculated from (21).

To verify the proposed design method, a design example is given: If the upper and lower boundaries of PM and GM is chosen as $15° \le \text{PM} \le 40°$ and $3\text{ dB} \le \text{GM} \le 20\text{ dB}$, respectively, and the magnitude error E_A is set to be less than 0.2%. Based on (28) and (30), all the possible K_c and f_c under different delay conditions are plotted in the shaded area in Fig. 11. The delay T_d exists in the expression of $K_{c,\text{PM}}$ in (28), thus the delay time affects the phase margin of the system. As can be seen from Fig. 11, from the minimum delay time to maximum delay time, the satisfactory region moves towards to the lower frequency.

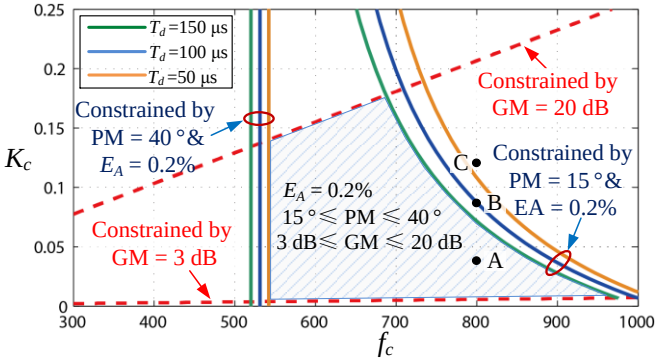

Fig. 11. Region of f_c and K_c constrained by GM, PM and E_A.

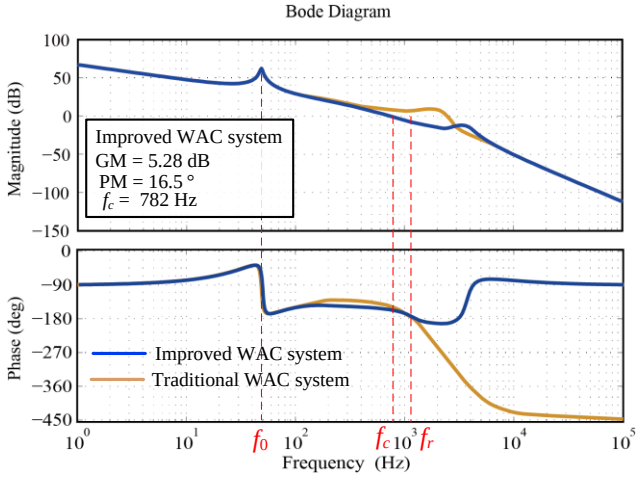

Fig. 12. Bode plots of the improved WAC feedback system with the designed parameters.

Therefore, K_c and f_c should be selected inside the shaded area to ensure the system stability under different delay conditions.

From Fig. 11, point A is selected with f_c=800 Hz and K_c=0.03. With (22), the calculated proportional gain K_p is 0.028. Substituting K_c, K_p and E_A into (21), K_r= 36.5 can be obtained. Considering the previous steps, the designed parameters can be obtained as:

$$K_c = 0.03, K_p = 0.028, K_r = 36.5 \qquad (31)$$

Based on the parameters in (31), the system bode plots is shown in Fig. 12. The gain margin (GM) is 5.28 dB, the phase margin (PM) is 16.5 °and the crossover frequency f_c is 782 Hz, all satisfying the aforementioned specifications, which are consistent with the theoretical analysis.

The variation tendencies of traditional and improved WAC system performance indexes, PM, GM and f_c, with respect to the system delay T_d variation are depicted in Fig. 13. In Fig. 13, PM, PM and f_c all decrease when T_d increases, the stability and transient responses of the system will be inevitably worse. However, when T_d increases from the minimum delay time (50 μs) to maximum delay time (150 μs), the improved WAC system remains stable while the traditional WAC system becomes unstable. Therefore, with capacitor current feedback, the WAC system become more robust against time delay.

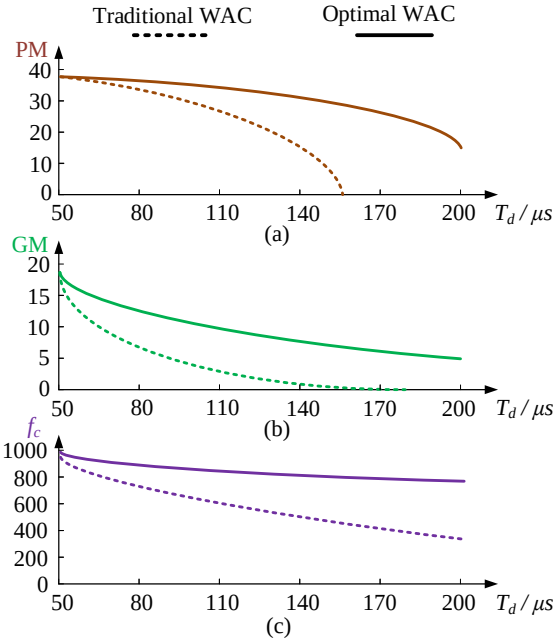

Fig. 13. Variation tendencies of PM, GM and f_c when T_d increases. (a) Variation tendencies of PM when T_d increases, (b) Variation tendencies of GM when T_d increases, and (c) Variation tendencies of f_c when T_d increases.

To further validate the effectiveness of the proposed design method, simulation results with T_d=100 μs and different K_c are presented in Fig. 14. Different K_c are selected in Fig. 11, With K_c= 0.03, K_p=0.028 and K_r=36.5, which correspond to point A, are selected, the system is perfectly stable as shown in Fig. 14(a). The fundamental rms value of the injected grid current i_g is 2.002 A, the reference value is 2 A, thus the steady-state amplitude error is 0.1%. Fig. 14(b) shows dynamic response when the reference of reference current jump from 2 A to 4 A. The percentage overshoot (PO) is 5%, and the settling time is about 0.3 ms. With K_c= 0.08, K_p=0.028 and K_r=36.5, which correspond to point B, are selected, on the edge of the satisfactory margin, the system remains stable, but there are small oscillations on the waveforms in Fig. 14(c). With K_c= 0.12, K_p=0.028 and K_r=36.5 selected in point C, which is out of the satisfactory region, the system cannot work in stable state in Fig.14(d). Hence the simulation results verified the correctness of the proposed design method.

Therefore, with the designed controller and active damping parameters, both the system stability and dynamic response can be ensured.

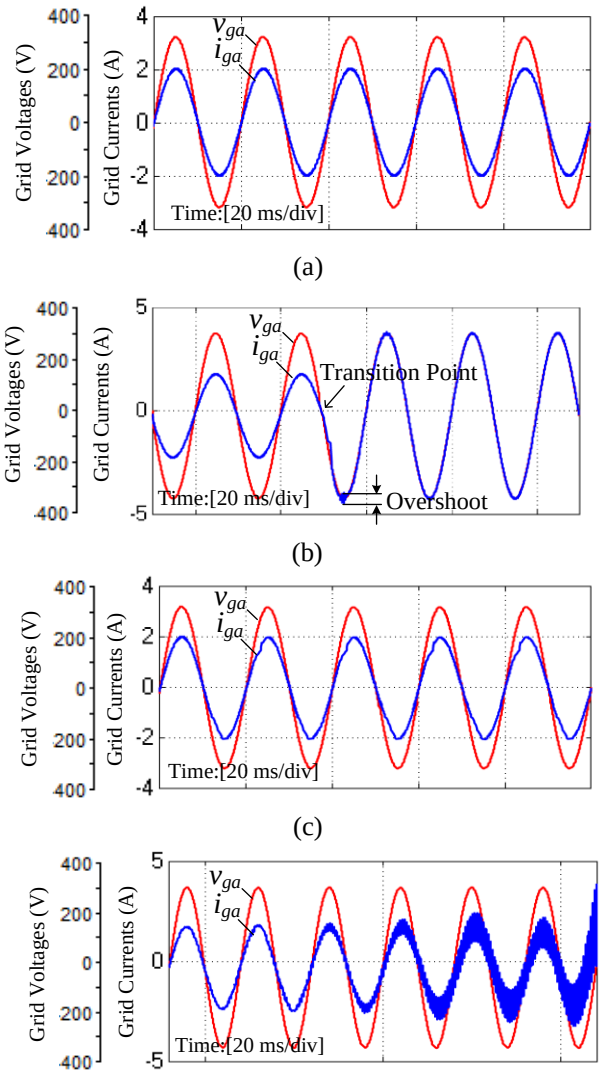

Fig. 14. Simulation results of improved WAC control with different capacitor current feedback coefficients (only phase-A voltage and current are shown) (a) Steady state response at point A with K_c= 0.03 (b) Dynamic response at point A (c) At point B with K_c= 0.08 and (d) At point C with K_c= 0.12.

IV. Experimental Results and Discussions

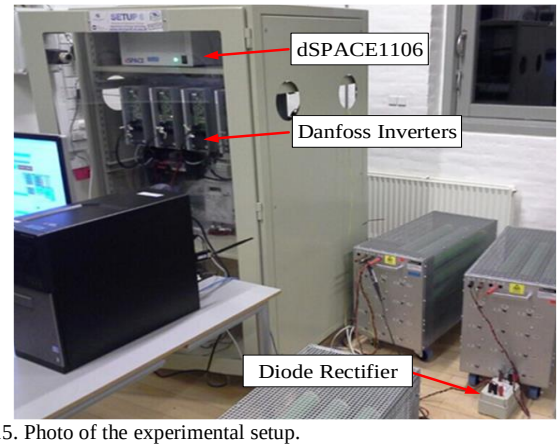

Fig. 15. Photo of the experimental setup.

To validate the analysis, the current control strategies are evaluated on a 2.2 kW three-phase experimental platform based on Dansfoss inverter, as shown in Fig. 15. The experimental setup was built and tested in the Microgrid Research Lab of Aalborg University[29], and the parameters of the power stage and controllers are consistent with the theoretical analysis.

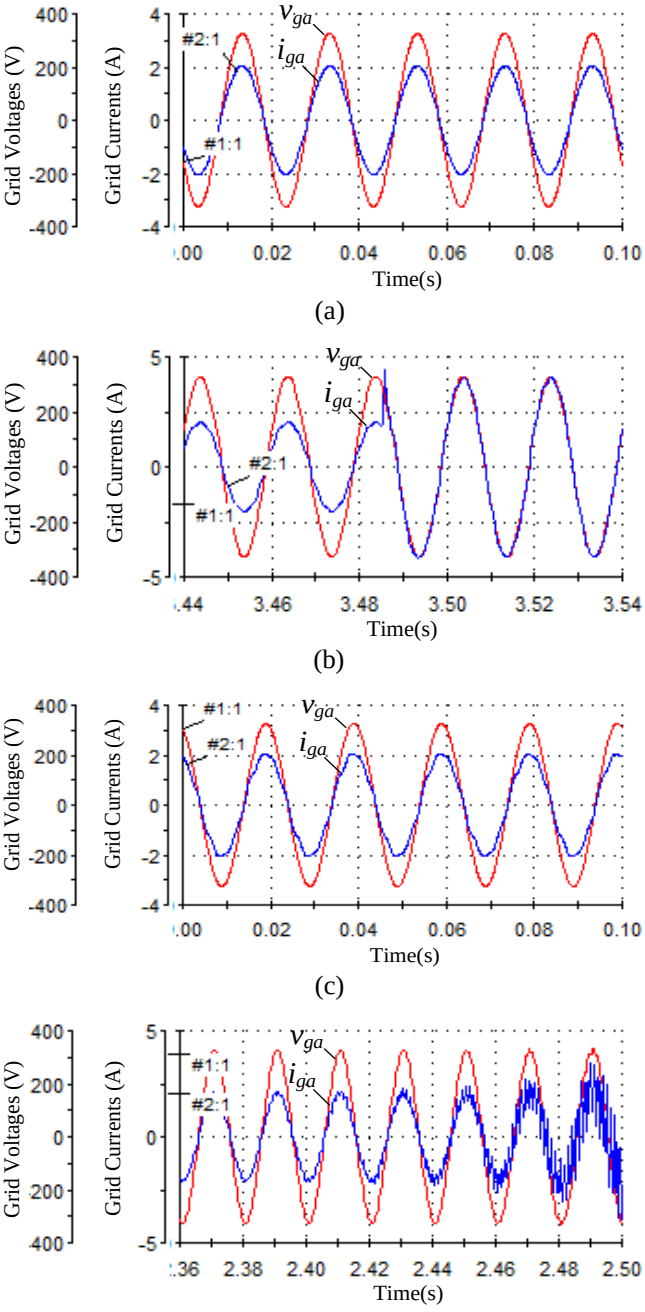

Fig. 16. Experimental results of improved WAC control system with different capacitor current feedback coefficients (only phase-A voltage and current are shown) (a)Steady state response at point A with K_c= 0.03 (b) Dynamic response at point A (c) At point B with K_c= 0.08 and (d) At point C with K_c= 0.12.

Fig. 16 shows the experimental waveforms of the improved WAC feedback control scheme with different capacitor current feedback coefficients. With K_c= 0.03, K_p=0.028 and K_r=36.5 which corresponds to point A in Fig. 11, the grid current oscillation is relatively small and the dynamic performance is also satisfactory, which verified the excellent performance of the improved WAC control under normal grid condition. With

K_c= 0.08 which correspond to point B are selected, the system is still in stable state, but there are obvious distortion in the grid current waveforms in Fig. 16(c). In Fig. 16(d), with K_c= 0.12 selected in point C, which is out of the satisfactory region, the

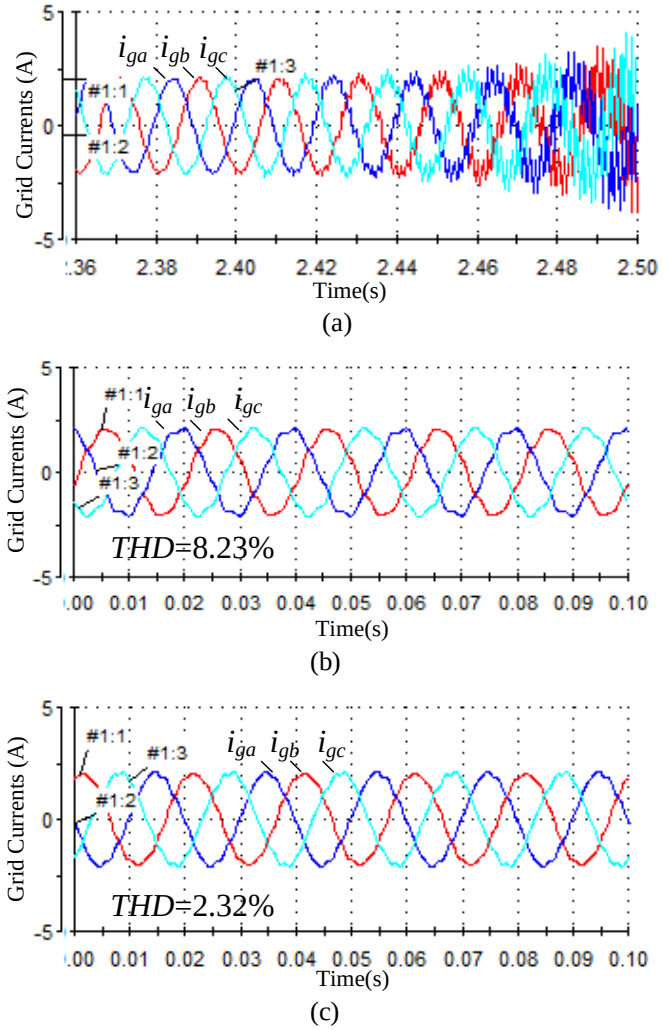

Fig. 17. Experimental waveforms with 1.2 mH grid impedance: (a) Grid currents of the grid-side current feedback control scheme. (b) Grid currents of the traditional WAC feedback control scheme. (c) Grid currents of the improved WAC feedback control scheme.

system cannot work in stable state. Therefore, the experimental waveforms well match the simulation waveforms as shown in Fig. 14.

Fig. 17 shows the experimental results under weak grid conditions when the grid inductance is approximately 1.2 mH. In Fig. 17(a), when the i_g plus i_c current feedback control method is used, the system become unstable with a high current loop gain under weak grid scenario. In Fig. 17(b), the current is distorted with the THD of 8.32% under traditional WAC feedback control, and the system is still in stable state. Fig. 17(c) shows the experimental results for the improved WAC control scheme under weak grid scenario.

By improving the robustness against the grid impedance variation and eliminating the resonance effect, the THD of grid current is reduced to 2.32%, and the quality of the grid currents are significantly improved. The results verify the effectiveness of the proposed improved WAC control scheme under weak grid conditions, which can be preferred in the grid-integration of DGs to the weak grid conditions.

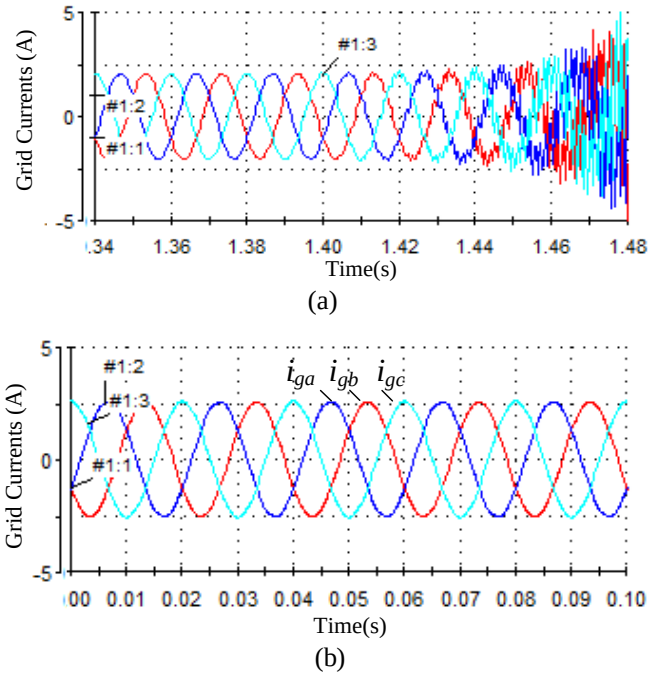

Fig. 18. Experimental waveforms with approximately 150 μs delay time: (a) Grid currents of the traditional WAC feedback control scheme. (b) Grid currents of the improved WAC feedback control scheme.

Fig. 18 shows the experimental results with approximately 150 μs delay time, when the control parameters are consistent with the analysis in the previous section. It can be seen from Fig. 18, the system with traditional WAC feedback method becomes unstable with an increased delay time of about 150 μs. Under the capacitor current feedback, the system with improved WAC method is still stable. Therefore, the robustness of the improved WAC method against time delay has been verified.

V. Conclusion

This paper investigates the active damping characteristics and system stability of weighted average current feedback control method. Compared with traditional grid current plus capacitor current feedback control scheme, the improved WAC feedback control method is capable to provide larger bandwidth at higher frequencies, and has higher robustness against the grid impedance variation.

In order to achieve optimal system performance, a systematic parameter design guideline for optimal selection of the current loop PR controller and the additional capacitor current feedback coefficients is presented. The satisfactory range of the system control parameters can be obtained under different control delay conditions to meet the system specifications. The improved WAC method enhances system robustness under weak grid scenarios, and the system become more robust against time delay, thus system stability and performance are remarkably improved. The experimental results are presented to validate the effectiveness of the improved WAC control scheme and parameter design methodologies, which can be widely applied for the grid-integration of DGs to the grid with a long transmission cable with a large equivalent grid impedance and distorted grid voltage conditions.

REFERENCES

[1] B. Gu, J. Dominic, J. S. Lai, C. L. Chen, T. LaBella and B. Chen, "High Reliability and Efficiency Single-Phase Transformerless Inverter for Grid-Connected Photovoltaic Systems," *IEEE Trans. Power Electron*, vol. 28, no. 5, pp. 2235-2245, May 2013.

[2] A. Reznik, M. G. Simões, A. Al-Durra and S. M. Muyeen, " LCL Filter Design and Performance Analysis for Grid-Interconnected Systems," *IEEE Trans. Ind. Appl*, vol. 50, no. 2, pp. 1225-1232, March-April 2014.

[3] X. Wang, F. Blaabjerg and P. C. Loh, "Virtual RC Damping of LCL-Filtered Voltage Source Converters With Extended Selective Harmonic Compensation," *IEEE Trans. Power Electron*, vol. 30, no. 9, pp. 4726-4737, Sept. 2015.

[4] W. Wu, Y. He, T. Tang and F. Blaabjerg, "A New Design Method for the Passive Damped LCL and LLCL Filter-Based Single-Phase Grid-Tied Inverter," *IEEE Trans. Ind. Electron*, vol. 60, no. 10, pp. 4339-4350, Oct. 2013.

[5] J. Dannehl, C. Wessels and F. W. Fuchs, "Limitations of Voltage-Oriented PI Current Control of Grid-Connected PWM Rectifiers With LCL Filters," *IEEE Trans. Ind. Electron*, vol. 56, no. 2, pp. 380-388, Feb. 2009.

[6] D. Pan, X. Ruan, C. Bao, W. Li and X. Wang, "Capacitor-Current-Feedback Active Damping With Reduced Computation Delay for Improving Robustness of LCL-Type Grid-Connected Inverter," *IEEE Trans. Power Electron*, vol. 29, no. 7, pp. 3414-3427, July 2014.

[7] Z. Bai, H. Ma, D. Xu, B. Wu, Y. Fang and Y. Yao, "Resonance Damping and Harmonic Suppression for Grid-Connected Current-Source Converter," IEEE Trans. Ind. Electron, vol. 61, no. 7, pp. 3146-3154, July 2014.

[8] Z. Xin, P. C. Loh, X. Wang, F. Blaabjerg and Y. Tang, "Highly Accurate Derivatives for LCL-Filtered Grid Converter With Capacitor Voltage Active Damping," *IEEE Trans. Power Electron*, vol. 31, no. 5, pp. 3612-3625, May 2016.

[9] Q. C. Zhong; G. C. Konstantopoulos, "Current-Limiting Droop Control of Grid-connected Inverters," *IEEE Trans. Ind. Electron*, vol.PP, no.99, pp.1-1

[10] S. G. Parker, B. P. McGrath and D. G. Holmes, "Regions of Active Damping Control for LCL Filters," *IEEE Trans. Ind. Appl*, vol. 50, no. 1, pp. 424-432, Jan.-Feb. 2014.

[11] Poh Chiang Loh and D. G. Holmes, "Analysis of multiloop control strategies for LC/CL/LCL-filtered voltage-source and current-source inverters," *IEEE Trans. Ind. Appl*, vol. 41, no. 2, pp. 644-654, March-April 2005.

[12] A. A. A. Radwan and Y. A. R. I. Mohamed, "Power Synchronization Control for Grid-Connected Current-Source Inverter-Based Photovoltaic Systems," *IEEE Trans. Energy Convers*, vol. 31, no. 3, pp. 1023-1036, Sept. 2016.

[13] Y. Jia, J. Zhao and X. Fu, "Direct Grid Current Control of LCL-Filtered Grid-Connected Inverter Mitigating Grid Voltage Disturbance," *IEEE Trans. Power Electron*, vol. 29, no. 3, pp. 1532-1541, March 2014.

[14] X. Zhang, J. W. Spencer and J. M. Guerrero, "Small-Signal Modeling of Digitally Controlled Grid-Connected Inverters With LCL Filters," IEEE Trans. Ind. Electron, vol. 60, no. 9, pp. 3752-3765, Sept. 2013.

[15] C. Bao, X. Ruan, X. Wang, W. Li, D. Pan and K. Weng, "Step-by-Step Controller Design for LCL-Type Grid-Connected Inverter with Capacitor–Current-Feedback Active-Damping," *IEEE Trans. Power Electron*, vol. 29, no. 3, pp. 1239-1253, March 2014.

[16] J. He and Y. W. Li, "Generalized Closed-Loop Control Schemes with Embedded Virtual Impedances for Voltage Source Converters with LC or LCL Filters," *IEEE Trans. Power Electron*, vol. 27, no. 4, pp. 1850-1861, April 2012.

[17] Y. Han, Z. Li and J. M. Guerrero, "Dynamic evaluation of LCL-type grid-connected inverters with different current feedback control schemes," 2015 9th International Conference on Power Electronics and ECCE Asia (ICPE-ECCE Asia), Seoul, 2015, pp. 391-396.

[18] N. He et al., "Weighted Average Current Control in a Three-Phase Grid Inverter With an LCL Filter," *IEEE Trans. Power Electron*, vol. 28, no. 6, pp. 2785-2797, June 2013.

[19] G. Shen, X. Zhu, J. Zhang and D. Xu, "A New Feedback Method for PR Current Control of LCL-Filter-Based Grid-Connected Inverter," *IEEE Trans. Ind. Electron*, vol. 57, no. 6, pp. 2033-2041, June 2010.

[20] M. S. Munir, J. He and Y. W. Li, "Comparative analysis of closed-loop current control of grid connected converter with LCL filter," 2011 IEEE International Electric Machines & Drives Conference (IEMDC), Niagara Falls, ON, 2011, pp. 1641-1646.

[21] D. Pan, X. Ruan, X. Wang, H. Yu, Z. Xing, "Analysis and Design of Current Control Schemes for LCL-Type Grid-Connected Inverter Based on a General Mathematical Model," *IEEE Trans. Power Electron*, vol.PP, no.99, pp.1-1

[22] J. Xu and S. Xie, "Optimization of weighted current control for grid-connected LCL-filtered inverters," 2013 IEEE ECCE Asia Downunder, Melbourne, VIC, 2013, pp. 1170-1175.

[23] D. Pan, X. Ruan, C. Bao, W. Li and X. Wang, "Optimized Controller Design for LCL -Type Grid-Connected Inverter to Achieve High Robustness Against Grid-Impedance Variation," *IEEE Trans. Ind. Electron*, vol. 62, no. 3, pp. 1537-1547, March 2015.

[24] X. Li, X. Wu, Y. Geng, X. Yuan, C. Xia and X. Zhang, "Wide Damping Region for LCL-Type Grid-Connected Inverter With an Improved Capacitor-Current-Feedback Method," *IEEE Trans. Power Electron*, vol. 30, no. 9, pp. 5247-5259, Sept. 2015.

[25] M. Huang, X. Wang, P. C. Loh and F. Blaabjerg, "Active damping of LLCL-filter resonance based on LC-trap voltage and capacitor current feedback," 2015 IEEE Applied Power Electronics Conference and Exposition (APEC), Charlotte, NC, 2015, pp. 2903-2910.

[26] X. Wang, C. Bao, X. Ruan, W. Li and D. Pan, "Design Considerations of Digitally Controlled LCL-Filtered Inverter With Capacitor-Current-Feedback Active Damping," IEEE Journal of Emerging and Selected Topics in Power Electronics, vol. 2, no. 4, pp. 972-984, Dec. 2014.

[27] J. L. Agorreta, M. Borrega, J. López and L. Marroyo, "Modeling and Control of N -Paralleled Grid-Connected Inverters With LCL Filter Coupled Due to Grid Impedance in PV Plants," *IEEE Trans. Power Electron*, vol. 26, no. 3, pp. 770-785, March 2011.

[28] J. Xu, S. Xie and T. Tang, "Evaluations of current control in weak grid case for grid-connected LCL-filtered inverter," in IET Power Electronics, vol. 6, no. 2, pp. 227-234, Feb. 2013.

[29] "(Jul. 2014). Microgrid Research Programme, Aalborg University. [Online]. Available: http://www.microgrids.et.aau.dk."

Yang Han (S'08-M'10) received the B.S. degree in Electrical Engineering from University of Electronic Science and Technology of China (UESTC), Chengdu, China, in 2004, and received the Ph.D. in Electrical Engineering from Shanghai Jiaotong University (SJTU), Shanghai, China, in 2010. He has been an Associate Professor since 2013. From March 2014 to March 2015, he was a visiting scholar in the area of renewable energy and microgrids at the Department of Energy Technology, Aalborg University, Aalborg, Denmark.

His research interests include AC/DC microgrids, grid-connected converters for renewable energy systems and DGs, power quality, multilevel PWM converters, active power filters and static synchronous compensators for smart grid applications. He has served as the Session Chair in "AC/DC, DC/AC Power Converter" session in the IPEMC 2016-ECCE Asia in Hefei, China. He was awarded "2016 Baekhyun Award" for his contribution to the field of power electronics by the Korean Institute of Power Electronics (KIPE).

Zipeng Li received the B. S. degree in electrical engineering and automation from Sichuan Normal University, Chengdu, China, in 2014. He is currently working toward the M. S. degree in power electronics and electric drive from UESTC, Chengdu, China.

His current research interests include the modelling and control of power electronics, multilevel converters, digital signal processing (DSP), and digital simulation of the grid-connected PV power plants.

Ping Yang received the B.S. in Mechanical Engineering from Shanghai Jiaotong University (SJTU), Shanghai, China, in 1984, and the M. S. in Mechanical Engineering from Sichuan University in 1987, respectively. He is currently a full professor with the School of Mechatronics Engineering, University of Electronic Science and Technology of China (UESTC), Chengdu, China. He was visiting the Victory University, Australia from July 2004 to August 2004, and a visiting scholar with the S. M. Wu Manufacturing Research Center, University of Michigan, Ann Arbor, USA, from August 2009 to February 2010, and was visiting the University of California, Irvine, USA, from October 2012 to November 2012.

His research includes mechatronics engineering, electrical engineering and automation, computer-aided control and instrumentation, smart mechatronics, and detection and automation of mechanical equipment. He has authored more than 60 papers in various journals and international conferences, and several books on mechatronics and instrumentation. He received several provincial awards for his contribution in teaching and academic research. He is currently the Dean of the School of Mechatronics Engineering, UESTC.

Congling Wang received the B. S. degree from Nanjing University of Aeronautics and Astronautics, Nanjing, China, in 1991, and the M. S. in University of Electronic Science and Technology of China (UESTC), Chengdu, China, in 1996. Since 1996, he has been a faculty member of the School of Mechatronics Engineering, and is currently an Associate Professor of UESTC.

His research includes the mechatronics engineering, electrical engineering and automation, computer-aided control and instrumentation, smart mechatronics, and detection and automation of mechanical equipment.

Lin Xu received the Ph.D. degree in Electrical Engineering from Shanghai JiaoTong University (SJTU), Shanghai, China, in 2011. Currently, she is a Senior Engineering at Sichuan Electric Power Research Institute, State Grid Sichuan Electric Power Company, Chengdu, China. She has co-authored more than 20 journal and conference papers in the area of power electronics and power systems.

Her research interests include power quality, power system analysis and real-time digital simulator (RTDS), flexible Ac transmission systems (FACTS), such as STATCOMs and power quality conditioners (DVRs, APFs). She is an active reviewer for IEEE Transactions on Industrial Electronics, IEEE Transactions on Power Electronics, Electric Power Components and Systems, etc.

Josep M. Guerrero (S'01-M'04-SM'08-FM'15) received the B.S. degree in telecommunications engineering, the M.S. degree in electronics engineering, and the Ph.D. degree in power electronics from the Technical University of Catalonia, Barcelona, in 1997, 2000 and 2003, respectively. Since 2011, he has been a Full Professor with the Department of Energy Technology, Aalborg University, Denmark, where he is responsible for the Microgrid Research Program (www.microgrids.et.aau.dk). From 2012 he is a guest Professor at the Chinese Academy of Science and the Nanjing University of Aeronautics and Astronautics; from 2014 he is chair Professor in Shandong University; from 2015 he is a distinguished guest Professor in Hunan University; and from 2016 he is a visiting professor fellow at Aston University, UK, and a guest Professor at the Nanjing University of Posts and Telecommunications.

His research interests is oriented to different microgrid aspects, including power electronics, distributed energy-storage systems, hierarchical and cooperative control, energy management systems, smart metering and the internet of things for AC/DC microgrid clusters and islanded minigrids; recently specially focused on maritime microgrids for electrical ships, vessels, ferries and seaports. Prof. Guerrero is an Associate Editor for the IEEE TRANSACTIONS ON POWER ELECTRONICS, the IEEE TRANSACTIONS ON INDUSTRIAL ELECTRONICS, and the IEEE Industrial Electronics Magazine, and an Editor for the IEEE TRANSACTIONS on SMART GRID and IEEE TRANSACTIONS on ENERGY CONVERSION. He has been Guest Editor of the IEEE TRANSACTIONS ON POWER ELECTRONICS Special Issues: Power Electronics for Wind Energy Conversion and Power Electronics for Microgrids; the IEEE TRANSACTIONS ON INDUSTRIAL ELECTRONICS Special Sections: Uninterruptible Power Supplies systems, Renewable Energy Systems, Distributed Generation and Microgrids, and Industrial Applications and Implementation Issues of the Kalman Filter; the IEEE TRANSACTIONS on SMART GRID Special Issues: Smart DC Distribution Systems and Power Quality in Smart Grids; the IEEE TRANSACTIONS on ENERGY CONVERSION Special Issue on Energy Conversion in Next-generation Electric Ships. He was the chair of the Renewable Energy Systems Technical Committee of the IEEE Industrial Electronics Society. He received the best paper award of the IEEE Transactions on Energy Conversion for the period 2014-2015, and the best paper prize of IEEE-PES in 2015. As well, he received the best paper award of the Journal of Power Electronics in 2016. In 2014, 2015, and 2016 he was awarded by Thomson Reuters as Highly Cited Researcher, and in 2015 he was elevated as IEEE Fellow for his contributions on "distributed power systems and microgrids."